TEMPORAL DYNAMICS OF VORTICAL STRUCTURES IN TURBULENT CHANNEL FLOW

Giancarlo Alfonsi
CESIC – Supercomputing Center for Computational Engineering
Università della Calabria
Via P. Bucci 22b, I-87036 Rende (Cosenza), Italy
giancarlo.alfonsi@unical.it

Leonardo Primavera
CESIC – Supercomputing Center for Computational Engineering
Università della Calabria
Via P. Bucci 22b, I-87036 Rende (Cosenza), Italy
lprimavera@fis.unical.it

ABSTRACT

The temporal dynamics of vortical structures in the wall region of turbulent channel flow is investigated. The Navier-Stokes equations are integrated numerically at friction Reynolds number $Re_\tau = 180$, using a computational code that utilizes a mixed spectral-finite difference technique and following the DNS approach.

A turbulent-flow database representing the turbulent statistically steady state of the velocity field through 10 viscous time units is computed and the method of the "imaginary part of the complex eigenvalue pair of the velocity-gradient tensor" is applied for vortex eduction.

Flow visualizations are provided that support a visual description of the evolutionary process with time of single and multiple hairpin vortical structures in the wall layer.

INTRODUCTION

The phenomena occurring in the wall region of turbulent shear flows have been investigated with different methods. One of the first results in studying the structure of the boundary layer is due to Kline et al. (1967) who showed that very near to the wall the flow organizes in alternating arrays of unsteady high- and low-speed regions aligned in the streamwise direction, called the *streaks*. Thereafter, much work has been accomplished.

Techniques for the detection of turbulent events have been introduced. Conditional sampling and averaging (Antonia, 1981), quadrant analysis (Willmarth and Lu, 1972), variable interval time averaging (Blackwelder and Kaplan, 1976) and also variable interval space averaging (Johansson et al., 1991) are examples of such techniques.

Vortical structures have been investigated. Theodorsen (1953) introduced the *hairpin* vortex model. Robinson (1991) confirmed the existence of *arch* vortices and *quasi-streamwise* vortices on the basis of DNS results. The composition of a quasi-streamwise vortex with an arch vortex may result in a hairpin vortex, but this result may strongly depend on the particular technique used for vortex detection. The most relevant processes of vortex interaction (with the surrounding ambient fluid and other vortices) are:

i) vortex compression and stretching in regions of increasing shear;

ii) spanwise vortex expansion and relaxation in regions of decreasing shear;

iii) vortex coalescence resulting in larger vortices;

iv) vortex reconnection into rings.

The leg of a vortex, considered in isolation, may appear as a quasi-streamwise vortex. The vortex head instead, rises through the flow field entering regions of decreasing shear. As a consequence, the vorticity in the vortex head diminishes (Head and Bandyopadhay, 1981).

The relation between vortical structures and turbulent events has been studied. The wall layer is subjected to a local breakdown and erupts into the outer region. Vorticity concentrated near the wall is ejected outward, the eruptive events providing new vorticity in the outer region. After the eruption, sweep events take place, in terms of high-speed fluid penetrating from upstream, close to the wall. The wall-layer breakdown is often interpreted as a viscous reaction of wall-layer fluid to the passage of hairpin vortices (Smith et al., 1991).

Conceptual models of boundary-layer turbulence based on vortex dynamics have also been provided by some authors (Willmarth and Tu, 1967, Offen and Kline, 1975, Praturi and Brodkey, 1978, Thomas and Bull, 1983, Acarlar and Smith, 1987, Robinson, 1991). Extensive reviews about boundary-layer turbulence can be found in Panton (2001) and Alfonsi (2006).

In spite of the amount of work accomplished, still there are no definite conclusions on the character of the phenomena occurring in the near-wall region of wall-bounded turbulent flows, mainly due to the fact that the majority of the results are based on flow visualizations or poitwise experimental measurements.

With the advent of DNS (Direct Numerical Simulation of turbulence) turbulent-flow databases of numerical nature became available, with the possibility of implementing

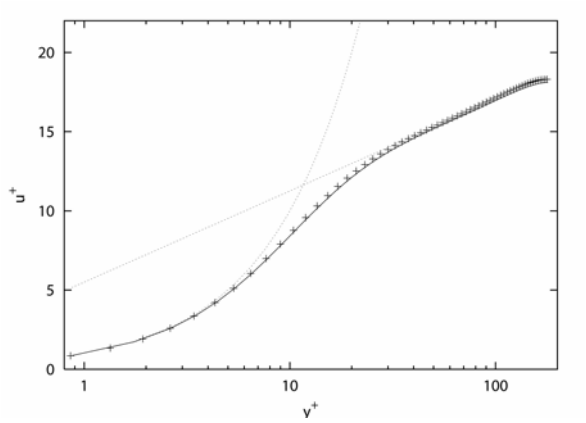

Figure 1. Mean velocity profile in wall coordinates: (—) present work; (+) data from Moser et al. (1999); (---) law of the wall $u^+ = y^+$, $u^+ = 2.5 ln\, y^+ + 5.5$

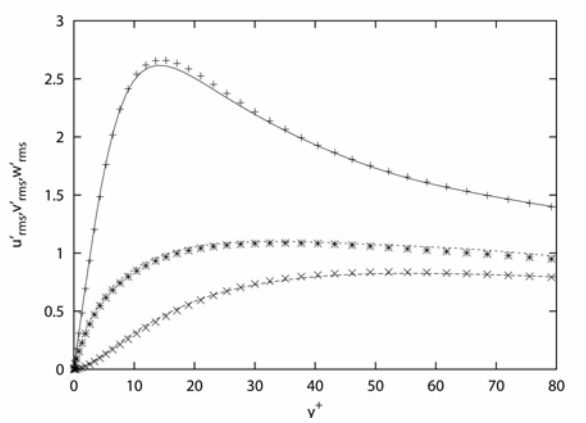

Figure 2. Rms velocity fluctuations in wall coordinates: (—) u'_{rms} , (---) v'_{rms} , (···) w'_{rms} , present work; (+) u'_{rms} , (×) v'_{rms} , (*) w'_{rms} , data from Moser et al. (1999)

mathematically-based definitions of flow structures for vortex eduction.

Mathematically-founded methods for the identification of vortical structures have been introduced by:

i) Perry and Chong (1987) based on the complex eigenvalues of the velocity-gradient tensor;

ii) Hunt et al. (1988) based on the second invariant of the velocity-gradient tensor;

iii) Zhou et al. (1999) based on the imaginary part of the complex eigenvalue pair of the velocity gradient tensor;

iv) Jeong and Hussain (1995) based on the analysis of the Hessian tensor of the pressure.

In the present work the issue of the evolution of vortical structures in the wall region of turbulent channel flow is addressed. The turbulent structures are educed from a DNS database that has been assembled by using a computational code that utlilizes a hybrid spectral-finite difference technique for the numerical integration of the unsteady three-dimensional Navier-Stokes equations at $Re_\tau = 180$.

The method used for vortex detection is that of the "imaginary part of the complex eigenvalue pair of the velocity-gradient tensor" of Zhou et al. (1999).

NUMERICAL SIMULATIONS

The unsteady Navier-Stokes equations for incompressible flow in nondimensional conservative form are considered ($i, j = 1,2,3$):

$$\frac{\partial u_i}{\partial t} + \frac{\partial}{\partial x_j}\left(u_i u_j\right) = -\frac{\partial p}{\partial x_i} + \frac{1}{Re_\tau}\frac{\partial^2 u_i}{\partial x_j \partial x_j} \qquad (1)$$

$$\frac{\partial u_i}{\partial x_i} = 0 \qquad (2)$$

where u_i is the velocity vector. Variables are nondimensionalized by the channel half-height h for lengths, wall-shear velocity $u_\tau = \sqrt{\tau_w/\rho}$ for velocities, ρu_τ^2 for pressure and h/u_τ for time, being $Re_\tau = u_\tau h/\nu$ the friction Reynolds number, ρ the fluid density and ν the fluid kinematic viscosity. The fields are admitted to be periodic in the streamwise (x) and spanwise (z) directions and equations (1-2) are Fourier transformed accordingly. The nonlinear terms in the momentum equations are evaluated pseudospectrally, by antitransforming the velocities back to physical space to perform the products (FFTs are used). A dealiasing procedure is applied to avoid errors in transforming the results back to Fourier space. To have a better spatial resolution near the walls, a grid stretching law of hyperbolic tangent type is introduced for the grid points along y , the direction normal to the solid walls. For time advancement, a third-order Runge-Kutta algorithm is implemented and time marching is accomplished with the fractional step method (Kim et al., 1987).

By recalling the wall formalism, one has: $x_i^+ = x_i u_\tau/\nu$, $t^+ = t u_\tau^2/\nu$, $u^+ = U/u_\tau$, where U denotes a *x*-velocity averaged on a *x*-*z* plane and time.

Table 1: Characteristic parameters of the simulations

computing domain					
L_x	L_y	L_z	L_x^+	L_y^+	L_z^+
$2\pi h$	$2h$	πh	1131	360	565

computational grid		
N_x	N_y	N_z
96	129	64

grid spacing			
Δx^+	Δy^+_{center}	Δy^+_{wall}	Δz^+
11.8	4.4	0.87	8.8

The characteristic parameters of the simulations are reported in Table 1. It can be verified that there are six grid points in the *y*-direction within the viscous sublayer ($y^+ \le 5$). The Kolmogorov spatial microscale, estimated using the criterion of the average dissipation rate per unit mass across the width of the channel, results $\eta^+ \approx 1.8$.

After the insertion of appropriate initial conditions, the initial transient of the flow in the channel is first simulated, the turbulent statistically steady state is reached and then calculated for a time $t = 10\,h/u_\tau$ ($t^+ = 1800$). 20000 time steps are computed with a temporal resolution of $5\times10^{-4}\,h/u_\tau$ ($\Delta t^+ = 0.09$). The estimated Kolmogorov time scale results $\tau \approx 1.89\times10^{-2}\,h/u_\tau$.

In Table 2 the predicted and computed values of a number of mean-flow variables are reported (U_b is the bulk velocity, Re_b is the related Reynolds number, U_c is the mean centerline velocity, Re_c the related Reynolds number). The predicted values of U_c/U_b and C_f reported in Table 2 are obtained from the experimental correlations suggested by Dean (1978):

$$\frac{U_c}{U_b} = 1.28\left(2\,Re_b\right)^{-0.0116} \tag{3}$$

$$C_f = 0.073\left(2\,Re_b\right)^{-0.25} \tag{4}$$

while the computed skin-friction coefficient:

$$C_f = \frac{2\tau_w}{\rho U_b^2} \tag{5}$$

where $\tau_w = \mu\left(\partial U/\partial y\right)_{wall}$, is calculated using the value of the shear stress at the wall actually obtained in the computations.

Table 2: Predicted vs. computed mean-flow variables

Re_τ	Re_b	Re_c	U_b/u_τ	U_c/u_τ	U_c/U_b	C_f
			predicted			
180	2800	3240	15.56	18.02	1.16	8.44×10^{-3}
			computed			
178.7	2786	3238	15.48	17.99	1.16	8.23×10^{-3}

In Figure 1, the mean-velocity profile normalized by the friction velocity in wall coordinates is compared with the data obtained by Moser et al. (1999) and with the law of the wall. In Figure 2, the rms velocity fluctuations normalized with the friction velocity in wall coordinates are compared with the data obtained by Moser et al. (1999). The agreement is rather satisfactory.

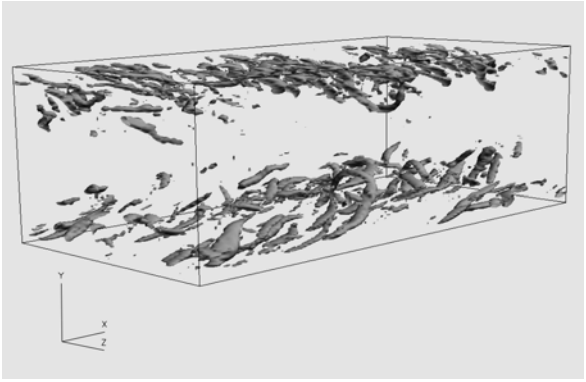

Figure 3. Vortical structures at $t^+ = 1036.8$

VORTEX-EDUCTION TECHNIQUE

By considering the Navier-Stokes equations, an arbitrary point O can be chosen in the flow field and a Taylor-series expansion of each velocity component can be performed in terms of the space coordinates, with the origin in O. One obtains:

$$u_i = A_i + A_{ij}x_j + A_{ijk}x_j x_k + ... \tag{6}$$

and the first-order approximation is:

$$u_i = A_i + A_{ij}x_j \tag{7}$$

If O is located at a critical point, the zero-order terms are equal to zero and:

$$A_{ij} = \frac{\partial u_i}{\partial x_j} \tag{8}$$

is the velocity-gradient tensor. From the characteristic equation of A_{ij} one has:

$$\lambda^3 + P\lambda^2 + Q\lambda + R = 0 \tag{9}$$

where:

$$P = -tr\left(\boldsymbol{A}\right) \tag{10}$$

$$Q = \frac{1}{2}\left(\left(tr\left(\boldsymbol{A}\right)\right)^2 - tr\left(\boldsymbol{A}^2\right)\right) \tag{11}$$

$$R = -det\left(\boldsymbol{A}\right) \tag{12}$$

are the scalar invariants of the velocity-gradient tensor (*tr* is trace, *det* is determinant). In incompressible fluids $P = 0$ and equation (9) becomes:

$$\lambda^3 + Q\lambda + R = 0 \tag{13}$$

where the discriminant of A_{ij} is defined as:

Figure 4. Single hairpin vortex at $t^+ = 1022.4$: *a)* top view; *b)* side view

Figure 5. Single hairpin vortex at $t^+ = 1051.2$: *a)* top view; *b)* side view

$$D = \left(\frac{R}{2}\right)^2 + \left(\frac{Q}{3}\right)^3 \tag{14}$$

When $D > 0$ the velocity-gradient tensor has one real eigenvalue (λ_1) and a pair of complex-conjugate eigenvalues (λ_2, λ_3). According to Zhou et al. (1999), isosurfaces of the imaginary part of the complex eigenvalue pair (actually the square of) can be used to visualize vortices. The method is frame independent and due to the fact that the eigenvalue is complex only in regions of local circular or spiralling streamlines, it automatically eliminates regions having vorticity but not local spiralling motion.

With reference to equation (13) and defining the quantities:

$$J = \left(-\frac{R}{2} + \sqrt{\frac{R^2}{4} + \frac{Q^3}{27}}\right)^{\frac{1}{3}} \tag{15}$$

$$K = \left(+\frac{R}{2} + \sqrt{\frac{R^2}{4} + \frac{Q^3}{27}}\right)^{\frac{1}{3}} \tag{16}$$

one has:

$$\lambda_2 = -\frac{J+K}{2} + \frac{J-K}{2}\sqrt{-3} \tag{17}$$

$$\lambda_3 = -\frac{J+K}{2} - \frac{J-K}{2}\sqrt{-3} \tag{18}$$

RESULTS

After the application of the vortex-detection technique, through the simulated time frame ($0 \le t^+ \le 1800$) a flow field appears populated by turbulent-flow structures adjacent to both the upper and lower wall of the domain.

In the temporal subframe $1008 \le t^+ \le 1080$ a hairpin-like vortical structure forms on the right side of the bottom wall. An overall view of this phenomenon at $t^+ = 1036.8$ is shown in Figure 3 (the flow goes from left to right).

Single Hairpin

Figures 4-5 show the morphological evolution of the hairpin vortex - considered in isolation - through four time steps.

At $t^+ = 1022.4$ (Figure 4*a*) the vortex is relatively small, with one leg shorter than the other and the head slightly oriented rightward. Moreover, the two legs are not parallel but convergent. Legs and neck (Figure 4*b*) are inclined at an angle with respect to the horizontal bottom plane, with the head entering regions of decreasing shear.

Figure 6: Multiple hairpin vortex at $t^+ = 1044$

Figure 7: Multiple hairpin vortex at $t^+ = 1047.6$

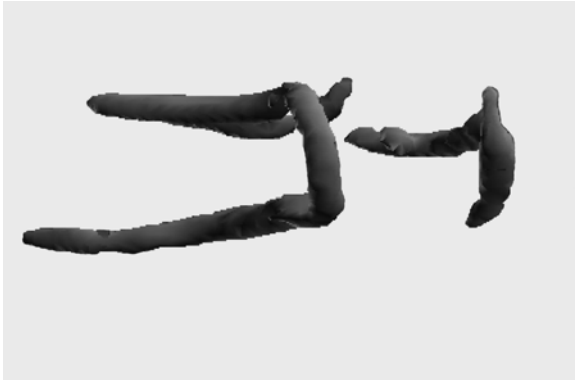

Figure 8: Multiple hairpin vortex at $t^+ = 1051.2$

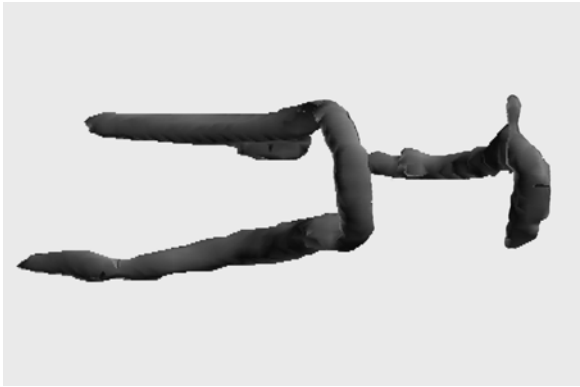

Figure 9: Multiple hairpin vortex at $t^+ = 1054.8$

At $t^+ = 1036.8$ (not shown) the vortex has increased its size and the legs are almost parallel, with one leg still shorter with respect to the other. The vortical structure grows, and the inclination of the neck is slightly larger with respect to the previous instant.

At $t^+ = 1051.2$ (Figure 5*a*) the size of the hairpin has increased considerably, both in the length of the two legs and in the height reached by the head. The angle at which the neck is inclined with respect to the bottom plane is slightly larger than that of the previous instants (Figure 5*b*).

At $t^+ = 1065.6$ (not shown) the process of growth of the hairpin vortex continues similarly to the instants previously considered. The legs become thinner due to vortex stretching near the wall. The head enters more deeply in regions of decreasing shear and expands in the spanwise direction.

Multiple Hairpin

Figures 6-9 show the evolution of a multiple-vortex configuration.

The upper leg of the primary hairpin is elongated along the streamwise direction past the primary hairpin itself and constitutes the nucleous for the formation of a smaller, secondary hairpin-like vortical structure. The secondary hairpin propagates downstream with about the same speed of the primary structure and, going from $t^+ = 1044$ to $t^+ = 1054.8$, its upper leg becomes more elongated. The neck of the secondary hairpin is swirled with in the *z*-direction (this is not visible from Figures 6-9) unveiling the secondary nature of its origin, with respect to the primary hairpin.

The above process of evolution of the multiple vortical structure is in close agreement with the process described by Zhou et al. (1999) in their work based on numerical simulations performed with a hairpin-vortex initial condition.

CONCLUDING REMARKS

A direct numerical simulation is performed in the case of the turbulent channel flow at $Re_\tau = 180$. A numerical database is assembled and the criterion of the "imaginary part of the complex eigenvalue pair of the velocity-gradient tensor" (Zhou et al., 1999) is applied for vortex eduction.

The results clearly show the characteristics of the evolutionary process of both single and multiple hairpin vortical structure, as educed by means of the aforementioned criterion.

LIST OF REFERENCES

Acarlar, M. S., and Smith, C. R., 1987, "A study of hairpin vortices in a laminar boundary layer. Part 2. Hairpin vortices generated by fluid injection", Journal of Fluid Mechanics, Vol. 175, pp. 43-83.

Alfonsi, G., 2006, "Coherent structures of turbulence: methods of eduction and results", Applied Mechanics Reviews, Vol. 59, pp. 307-323.

Antonia, R. A., 1981, "Conditional sampling in turbulence measurement", Annual Review of Fluid Mechanics, Vol. 13, pp. 131-156.

Blackwelder, R. F., and Kaplan, R. E., 1976, "On the wall structure of the turbulent boundary layer", Journal of Fluid Mechanics, Vol. 76, pp. 89-112.

Dean, R. B., 1978, "Reynolds number dependence of skin friction and other bulk flow variables in two-dimensional rectangular duct flow", ASME Journal of Fluids Engineering, Vol. 100, pp. 215-223.

Head, M. R., and Bandyopadhyay, P., 1981, "New aspects of turbulent boundary-layer structure", Journal of Fluid Mechanics, Vol. 107, pp. 297-338.

Hunt, J. C. R., Wray, A. A., and Moin, P., 1988, "Eddies, streams and convergence zones in turbulent flows", Proceedings, Summer Program, Center for Turbulence Research, NASA Ames/Stanford University, pp. 193-208.

Jeong, J., and Hussain, F., 1995, "On the definition of a vortex", Journal of Fluid Mechanics, Vol. 285, pp. 69-94.

Johansson, A. V., Alfredsson, P. H., and Kim, J., 1991, "Evolution and dynamics of shear-layer structures in near-wall turbulence", Journal of Fluid Mechanics, Vol. 224, pp. 579-599.

Kim, J., Moin, P., and Moser, R. D., 1987, "Turbulence statistics in fully developed channel flow at low Reynolds number", Journal of Fluid Mechanics, Vol. 177, pp. 133-166.

Kline, S. J., Reynolds, W. C., Schraub, F. A., and Rundstadler, P. W., 1967, "The structure of turbulent boundary layers", Journal of Fluid Mechanics, Vol. 30, pp. 741-773.

Moser, R. D., Kim, J., and Mansour, N. N., 1999, "Direct numerical simulation of turbulent channel flow up to $Re_\tau = 590$ ", Physics of Fluids, Vol. 11, pp. 943-945.

Offen, G. R., and Kline, S. J., 1975, "A proposed model of the bursting process in turbulent boundary layers", Journal of Fluid Mechanics, Vol. 70, pp. 209-228.

Panton, R. L., 2001, "Overview of the self-sustaining mechanisms of wall turbulence", Progress in Aerospace Science, Vol. 37, pp. 341-383.

Perry, A. E., and Chong, M. S., 1987, "A description of eddying motions and flow patterns using critical-point concepts", Annual Review of Fluid Mechanics, Vol. 19, pp. 125-155.

Praturi, A. K., and Brodkey, R. S., 1978, "A stereoscopic visual study of coherent structures in turbulent shear flow", Journal of Fluid Mechanics, Vol. 89, pp. 251-272.

Robinson, S. K., 1991, "Coherent motions in the turbulent boundary layer", Annual Review of Fluid Mechanics, Vol. 23, pp. 601-639.

Smith, C. R., Walker, J. D. A., Haidari, A. H., and Soburn, U., 1991, "On the dynamics of near-wall turbulence", Philosophical Transactions of the Royal Society of London, Vol. 336, pp. 131-175.

Theodorsen, T., 1952, "Mechanism of turbulence", Proceedings, 2nd Midwestern Fluid Mechanics Conference, Columbus, Ohio, pp. 1-18.

Thomas, A. S. W., and Bull, M. K., 1983, "On the role of wall-pressure fluctuations in deterministic motions in the turbulent boundary layer", Journal of Fluid Mechanics, Vol. 128, pp. 283-322.

Willmarth, W. W., and Lu, S. S., 1972, "Structure of the Reynolds stress near the wall", Journal of Fluid Mechanics, Vol. 55, pp. 65-92.

Willmarth, W. W., and Tu, B. J., 1967, "Structure of turbulence in the boundary layer near the wall", Physics of Fluids, Vol. 10, Supplements, pp. 134-137.

Zhou, J., Adrian, R. J., Balachandar, S., and Kendall, T. M., 1999, "Mechanisms for generating coherent packets of hairpin vortices in channel flow", Journal of Fluid Mechanics, Vol. 387, pp. 353-396.